IOP Publishing Journal of Micromechanics and Microengineering

J. Micromech. Microeng. **17** (2007) S38–S49 doi:10.1088/0960-1317/17/4/S03

A cellular automaton-based simulator for silicon anisotropic etching processes considering high index planes

Zai-fa Zhou, Qing-an Huang, Wei-hua Li and Wei Deng

Key Laboratory of MEMS of the Ministry of Education, Southeast University, Nanjing 210096, People's Republic of China

E-mail: hqa@seu.edu.cn

Received 15 September 2006, in final form 2 January 2007
Published 20 March 2007
Online at stacks.iop.org/JMM/17/S38

Abstract

This paper presents a novel 3D continuous cellular automaton (CA) model with high index planes such as (2 1 1), (3 1 1), (3 3 1) and (4 1 1) efficiently incorporated. A dynamic algorithm has also been developed to speed up the simulation process and reduce the memory usage. A 3D silicon anisotropic etching simulator, SEAES, has been implemented based on the 3D continuous CA model and the dynamic algorithm. The simulation results by SEAES have been found to be in good agreement with the experimental results, and the arbitrarily complex mask shapes and the merging of 3D etching profiles can be both efficiently and accurately handled. This is identified to be useful for the research of anisotropic etching technologies and the development of micro-electro-mechanical systems (MEMS) design.

(Some figures in this article are in colour only in the electronic version)

1. Introduction

As the complexity of micro-electro-mechanical systems (MEMS) devices increases, both optimization and control of fabrication technologies of MEMS become increasingly important. Fabrication process simulation plays an important role in timely market entry of MEMS products and the development of MEMS fabrication technologies. Silicon anisotropic wet chemical etching using potassium hydroxide (KOH), ethylenediamine-pyrocatecol-water (EDP), or tetramethyl ammonium hydroxide (TMAH) solutions, as one of the key manufacture techniques in MEMS fabrication, plays a critical role in the development of most MEMS devices [1, 2].

The anisotropic etching processes can be greatly improved and optimized if efficient and accurate simulation tools are used to predict the performance. Over the past 20 years, a variety of 3D anisotropic etching simulators have been developed, generally based on geometric models [3–7] or atomistic models [8–16]. In the geometric models, the resultant 3D profiles corresponding to different etching times are determined by geometric rules with the silicon substrate is treated as a continuous entity. Geometric models require a less computer memory compared with the atomistic models; however, one major disadvantage of geometric models is that they cannot efficiently process complex structures with merging features. In contrast, the atomistic models exhibit high efficiency and accuracy when handling arbitrarily complex mask shapes and merging 3D etching profiles. The atomistic models are generally divided into two classes: cellular automaton (CA) models [8–12] and Monte Carlo models [13–16]. Over the past 10 years, anisotropic etching simulations have been investigated using some atomistic models; however, the current atomistic models have their own disadvantages. It has been proved that the etching rate (removal probability) of a surface atom is related to its first nearest neighbors, which was directly linked to the atom, and the locations of these first nearest neighbors to the etching surface [8, 11]. Although this method works in the case that only low index planes appear during anisotropic etching processes, this method cannot precisely predict high index planes during convex undercut etching processes. Some researches considering the effect from first nearest and second nearest neighbors have been carried out using Monte Carlo models [15, 16]; these attempts, however, still found difficulties to accurately determine high index planes, which

will be discussed in this paper. The continuous CA model [12] does not generate an artificially roughened surface, which is very convenient to carry out some mechanical analyses of the simulation profiles using available finite element analysis tools or CA methods, but this model finds many difficulties to predict high index planes, except the (3 1 1) plane.

Compared with the Monte Carlo models, the inherent parallelism of the CA models, spatial homogeneity and locality of cell interactions allow the computational process to be easily partitioned for allocating in several processors, parallel processors or processors with high efficiency of parallel instructions execution. As parallel processing is becoming the development tendency of microprocessors, CA models will keep competitive in the area of silicon anisotropic etching simulations. Furthermore, increasing efforts have been poured into the research about structure analysis using the CA method in MEMS design [17, 18], so the simulations of fabrication processes such as silicon anisotropic etching, deposition and photolithography using CA methods make the seamless link of fabrication process simulations and structure performance analysis possible. Although Monte Carlo models allow for a better understanding of physics involved in the complex process of silicon anisotropic etching, and offer interesting insights into the study of surface roughness [15], since we target at the seamless link of fabrication process simulations and mechanical performance analysis of microstructures based on the CA method, we focus on continuous CA models for the simulations of silicon anisotropic etching processes.

This paper presents a novel 3D continuous CA model for the simulations of silicon anisotropic etching processes. High index planes, such as (2 1 1), (3 1 1), (3 3 1) and (4 1 1), etc, have been accurately incorporated into the novel 3D continuous CA model by considering the first nearest neighbors, the second nearest neighbors and their locations with respect to the etching surface, so the accuracy of the continuous CA model is significantly increased. A dynamic algorithm has also been developed to speed up the simulation process and reduce the memory usage. Based on the novel CA model and the dynamic algorithm, a 3D silicon anisotropic etching simulator (SEAES) has been successfully developed. SEAES stands for south east anisotropic simulator. Some simulation results by SEAES will be presented and compared with the experimental results to investigate the effectiveness and efficiency of the simulator.

2. The novel 3D continuous CA model

We have a spirit, inspired from the available analysis by Gosalvez *et al* [15, 16], to incorporate the effects from the first nearest neighbors and the second nearest neighbors in our model. Our approaches, however, do not focus on the descriptions of removal probabilities or etching rate functions for various crystal planes, but focus on the respective values of removal probabilities or etching rates of surface cells on various typical crystal planes. So in this way, this paper can be considered as an extension of the model by Than and Buttgenbach [8].

Some works [19–29] studying the reaction mechanisms of wet chemical etching have produced some interesting results, and some reasonable physical points have been included for the anisotropic etching models [8–16] based on these assumptions of etching mechanisms. These assumptions and models can be used to qualitatively explain some etching phenomena; they, however, are not yet accurately covering their exact mechanisms during silicon anisotropic etching processes. Generally speaking, these models are not accurate enough to predict etching performance when high index planes dominate the etching processes. For example, Than and Buttgenbach have presented a CA model for the simulations of silicon anisotropic etching processes, and in their model, the etching rate of a surface cell is dependent on the numbers of its first nearest neighbors and the locations of its first nearest neighbors with respect to the etching surface [8]. Although some researches have considered the effects from the first nearest and second nearest neighbors, these methods, however, have difficulties to accurately determine high index planes, or have difficulties to accurately determine more such high index planes [15]. With the comparisons of experimental and simulation results, Gosalvez *et al* have presented a model which can theoretically determine six planes [19, 30], and this is very useful to investigate the mechanisms of silicon anisotropic etching processes. This paper attempts to incorporate crystal planes into the simulation model to satisfy the accuracy requirements of engineering practice cases.

Ideas to develop CA models considering the effects from the second nearest neighbors, besides the effects from the first nearest neighbors, have been presented by several groups [8, 9], but eventually not selected for the significant barrier of computational costs. The computational speed and internal storage capacity of a computer have increased by orders of magnitude in recent years, so the simulation considering the effects from the second nearest neighbors, currently, becomes very practical. The novel 3D continuous CA model presented in this paper attempts to accurately incorporate high index planes, such as (2 1 1), (3 1 1), (3 3 1) and (4 1 1), etc, by considering not only the numbers of the first nearest neighbors and the second nearest neighbors, but also the locations of these first nearest and second nearest neighbors with respect to the etching surface. Note that the number of second nearest neighbor cells includes the number of direct second nearest neighbor cells, which are linked to a target cell directly through first nearest neighbors, and the number of the indirect nearest neighbor cells, which are not linked to the target cell through a first nearest cell. Detailed descriptions of direct and indirect second nearest neighbors are given by [19, 31]. Zubel has classified some high index planes according to various surface bond types to qualitatively study the mechanism of isopropyl alcohol (IPA) interaction with high index planes during silicon anisotropic etching processes [32]. In order to quantitatively study the silicon anisotropic etching processes under various etching conditions, we attempt to identify cell (atoms) configurations for different high index planes, and then to deduce the correspondence between the microscopic etching rates of these classified cells and the macroscopic etching rates of these planes in this paper.

A cellular automaton consists of cells with discrete variables, and the states at each cell are updated simultaneously based on the states of the cell and its neighboring cells at the discrete time steps, and according to a definite set of 'local rules'. For developing the novel 3D continuous CA model, the

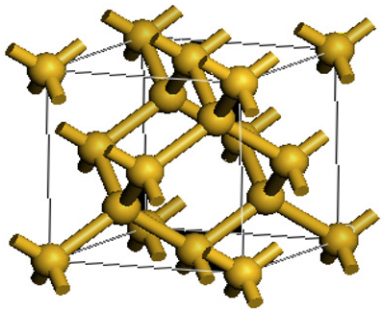

Figure 1. Silicon crystal structure.

diamond crystal structure of silicon is adopted as the lattice of the cellular automaton, as shown in figure 1. A silicon atom is represented by a cell in the model in terms of its lattice configuration, and the size of each cell depends on the selected resolution.

The crystal lattice representations of etching surfaces for the three low index planes are shown in figure 2. For a surface cell on the (1 0 0) plane, as shown in figure 2(*a*), it does not have first nearest surface neighbors but has two first nearest interior neighbors. Furthermore, it has four second nearest surface cells and four second nearest interior neighbors. An interior cell or neighbor means that it is not exposed to etching solutions, or in other words, none of its first nearest neighbors has been fully etched. For simplification, the cell configuration for the (1 0 0) plane can be simply notated as (0s, 2i, 4s, 4i), where 's' stands for surface, 'i' stands for interior, '0s' and '2i' are for the numbers of the first nearest surface neighbors and the first nearest interior neighbors, and '4s' and '4i' are for the numbers of the second nearest surface neighbors and the second nearest interior neighbors. Thus for a surface configuration on the (1 1 0) plane, the cell type should be notated as (2s, 1i, 2s, 5i), as shown in figure 2(*b*). Similarly, the cell type for a surface configuration on the (1 1 1) plane should be (0s, 3i, 6s, 3i), as shown in figure 2(*c*). Figure 3 shows crystal lattice representations of etching surface for (3 1 1) and (3 3 1) high index planes. The surface cell configurations on high index crystal planes can also be determined by the numbers of the first nearest surface neighbors, first nearest interior neighbors, second nearest surface neighbors and second nearest interior neighbors. For example, the cell configuration for a surface cell on the (3 1 1) plane should be (0s, 2i, 5s, 2i), as shown in figure 3(*b*). The numbers of first nearest and second nearest neighbors, and the locations of these first nearest and second nearest neighbors with respect to the etching surface for surface cells on some typical crystal planes have been summarized in table 1. From the table, we can see that if only the numbers of the first nearest neighbors and the second nearest neighbors [15, 16], but not their locations with respect to the etching surface, are considered, some typical planes will be considered as the same, for example, the (1 2 0) plane is the same as the (1 3 0) plane, (1 1 0) and (3 1 1) planes are the same as the (4 1 1) plane. This will inevitably reduce the simulation accuracy. As the locations of the first nearest neighbors and the second nearest neighbors with respect to the etching surface are also considered, almost all typical crystal planes, occurring during

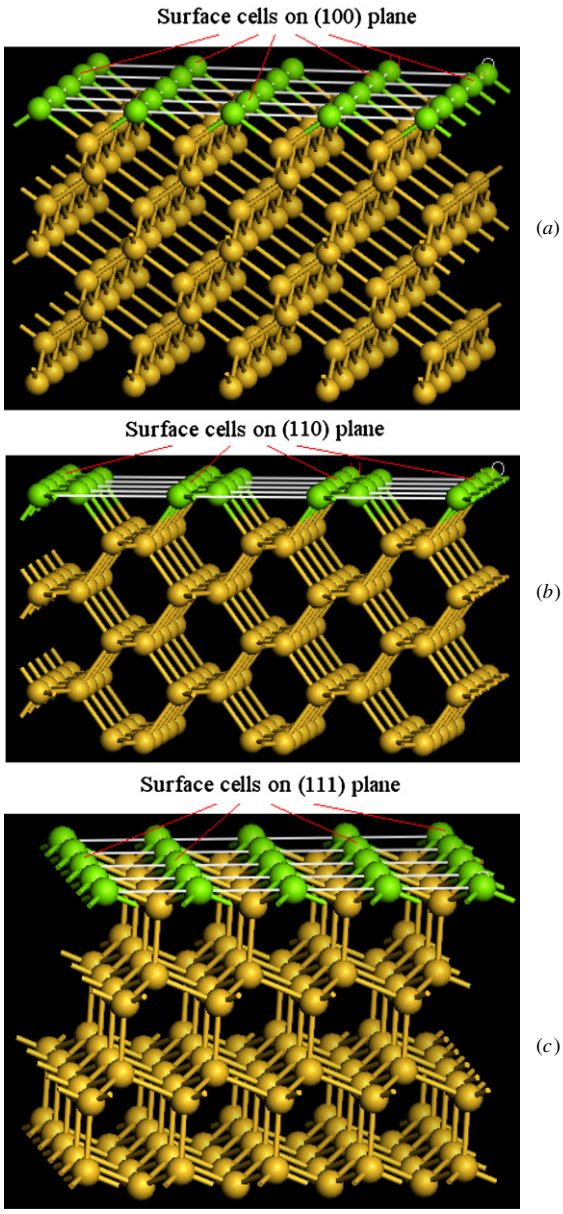

Figure 2. Bonding situations of the three low index surface cells in the novel 3D continuous CA model: (*a*), (*b*) and (*c*) are for surface cells on (1 0 0), (1 1 0) and (1 1 1) planes, respectively.

the silicon anisotropic etching process, can be determined by these cell configurations.

As mentioned above, our approaches focus on the respective microscopic etching rates for the classified cells on the typical crystal planes, as listed in table 1, based on the available macroscopic etching rates for these typical crystal planes; thus two problems deserve discussions. First, because the exact mechanisms during the etching process are still not fully understood for so many years after the development of the silicon anisotropic etching technology, many experimental researches have been carried out to obtain the etching data of silicon in different etching solution for the requirements of engineering applications [19–29, 31–43]. This is the background of our research, and the available etching rate data after many years of experimental research guarantee

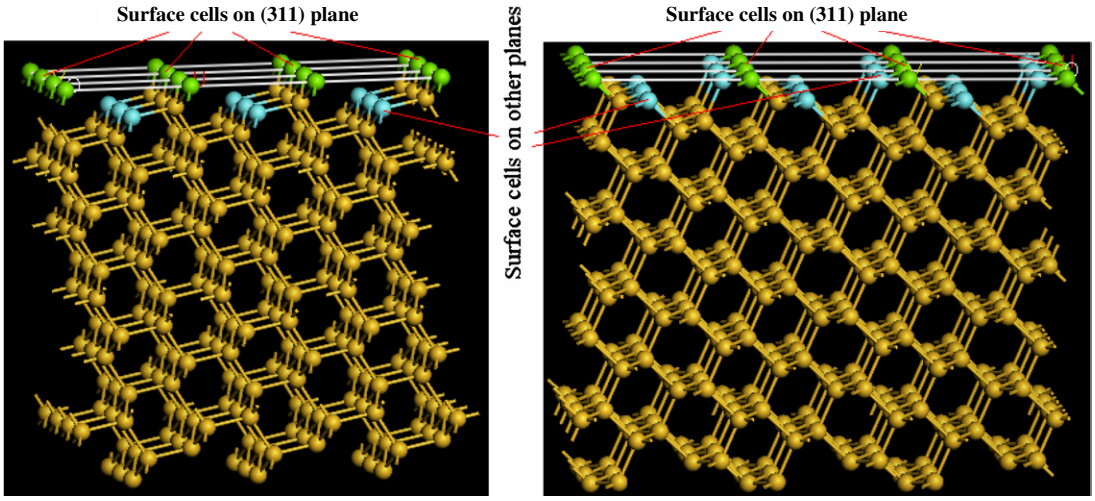

Figure 3. (*a*) and (*b*) are the bonding situations for surface cells on (3 1 1) and (3 3 1) planes, respectively.

Table 1. Numbers of the first nearest and second nearest neighbors and the locations of these first nearest and second nearest neighbors with respect to the etching surface for surface cells on some typical crystal planes.

Surface cells on some typical crystal planes	Numbers of unetched first nearest neighbors		Numbers of unetched second nearest neighbors	
	Surface cells	Interior cells	Surface cells	Interior cells
(1 0 0)	0	2	4	4
(1 1 0)	2	1	2	5
(1 1 1)	0	3	6	3
(1 2 0)	1	1	3	3
(1 3 0)	1	1	2	4
(2 1 1)	1	2	4	3
(3 1 1)	0	2	5	2
(3 3 1)	2	1	4	3
(4 1 1)	1	1	2	5

that our approaches are reasonable and practical. Second, the available etching rates for different crystal planes cannot directly be adopted as the etching rates of the surface cells as tabulated in table 1. For most crystal planes, there are some differences between the macroscopic etching rates for these crystal planes and the microscopic etching rates for the surface cells located on these crystal planes. Figures 4 and 5 show the side views of the crystal structure for some typical crystal planes. It is apparent that, for some crystal planes such as (3 1 1) and (3 3 1), the respective side view crystal structures are not simply repeated, and thus an efficient method should be developed to calculate the microscopic etching rates for different surface cells located on some typical crystal planes.

As the macroscopic etching rates for some typical crystal planes are determined, we assume that the microscopic etching rate for a surface cell with (as, bi, cs, di) configuration, as listed in table 1, can be summarized as

$$R_{(\mathrm{as,bi,cs,di})} = f(R_{100}, R_{110}, R_{111}, R_{120}, R_{130}, R_{211}, R_{311}, R_{331}, R_{411}). \quad (1)$$

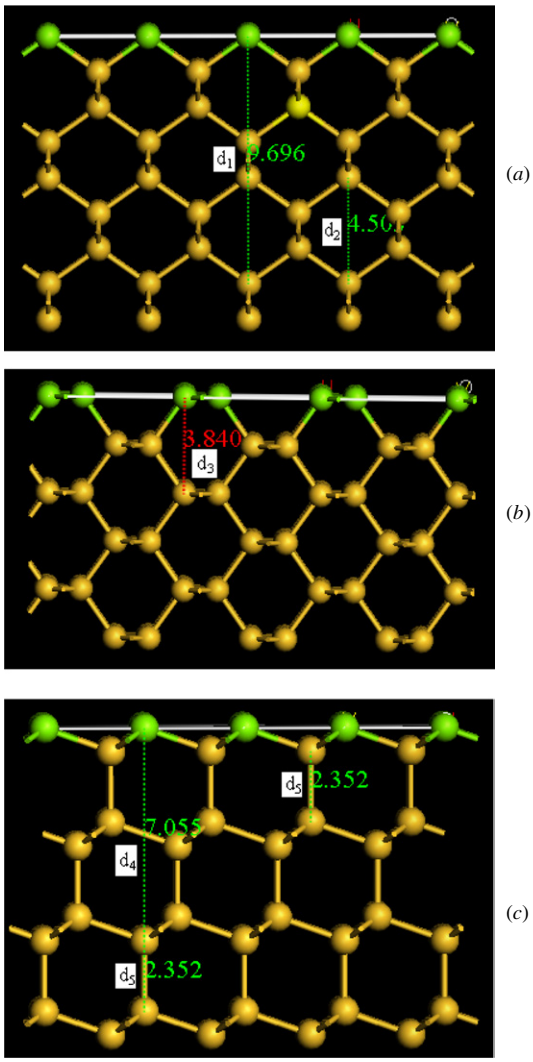

Figure 4. (*a*), (*b*) and (*c*) are the respective side views for (1 0 0), (1 1 0) and (1 1 1) wafers, respectively.

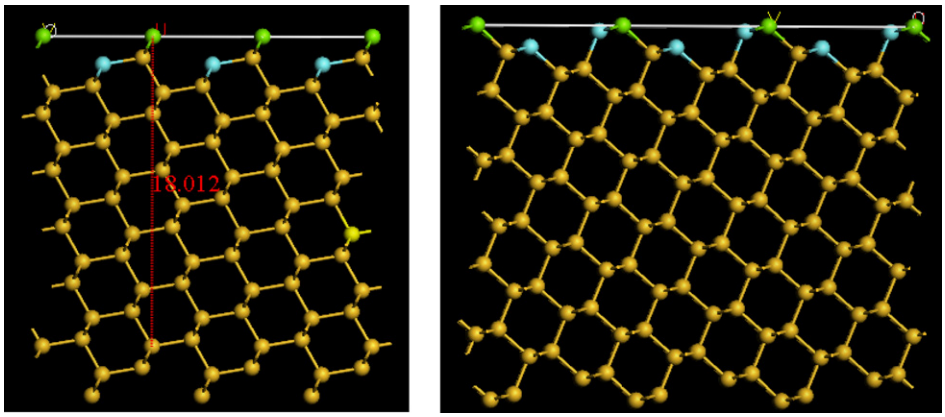

(*a*) (*b*)

Figure 5. (*a*) and (*b*) are the respective side views for (3 1 1) and (3 3 1) wafers, respectively.

Indices h, k, and l in R_{hkl} combine in such a way to refer to the macroscopic etching rate of (h k l) crystal planes. In our approaches, we determine the correspondence between the microscopic etching rates of these planes and the classified cells by individually etching different orientation silicon wafers. In this way, only several types of surface cells, even only one or two types of surface cells, will involved in the determination of the microscopic etching rate for certain cell configuration, as shown in figures 2–5; thus the fitting procedures have been significantly simplified, although they are still a little laboring intensive.

For example, since the respective side view crystal structures for (1 0 0) and (1 1 0) planes are simply repeated as shown in figures 4(*a*) and (*b*), the microscopic etching rates for surface cells on (1 0 0) and (1 1 0) planes can be directly determined using the corresponding macroscopic etching rates to begin our fitting procedures. The microscopic etching rate of a cell located on the (1 0 0) plane is $R_{(0s,2i,4s,4i)}$, the macroscopic etching rate of the (1 0 0) plane is R_{100}, the simulation scale factor is Re, and the state variable of the atom at the beginning of etching is 1, then

$$\frac{1}{R_{(0s,2i,4s,4i)}} \cdot 4 = \frac{(d_1 - d_2) \cdot \mathrm{Re}}{R_{100}} \tag{2}$$

where the simulation scale factor means that each cell in the simulation is Re times bigger than that of a real atom in silicon crystal. The definitions of d_1 and d_2 are shown in figure 4(*a*). So $R_{(0s,2i,4s,4i)}$ can be directly determined as

$$R_{(0s,2i,4s,4i)} = \frac{4R_{100}}{(d_1 - d_2) \cdot \mathrm{Re}}. \tag{3}$$

Similarly, the microscopic etching rate of a surface cell located on the (1 1 0) plane, $R_{(0s,2i,4s,4i)}$, can be directly determined using the macroscopic etching rate of the (1 1 0) plane R_{110}, as given by

$$R_{(2s,1i,2s,5i)} = \frac{2R_{110}}{d_3 \cdot \mathrm{Re}}. \tag{4}$$

The definition of d_3 in equation (4) is shown in figure 4(*b*).

After that, the microscopic etching rates for the surface cells on (1 1 1), (3 1 1) and (3 3 1) planes can be calculated by similar methods. Following that, the fitting procedures for determining the microscopic etching rates for surface cells on (2 1 1), (4 1 1), (1 2 0) and (1 3 0) planes can be implemented. Note that, in addition to the crystal planes listed in table 1, such special cases as singly bonded surface cells have also been considered in order to get the proper results by adjusting the corresponding microscopic etching rates according to the simulation results. The determination of microscopic etching rates for single-bonded cells and surface cells on some crystal planes such as (2 1 1), (4 1 1), (1 2 0) and (1 3 0) involves numerous comparisons of simulation and experimental results (including etching profiles and etching rates) to determine and adjust some relationships between surface cells with different cell configures to obtain the final microscopic etching rates. But after these relationships are determined, the corresponding microscopic etching rates for surface cells on different crystal planes will always be calculated according to these relationships, so that the calculated microscopic etching rates for surface cells on different crystal planes will be changed with the macroscopic etching rates changed under different etching conditions. The microscopic etching rates above are the mean etching rates, neglecting the morphologies of the etching surfaces. However, considering the simply repeated side view crystal structures of these planes, the inaccuracy caused by neglecting the morphologies of the etching surfaces can also be neglected for the simulations with the etching depth is greater than several micrometers.

Besides what is mentioned above, not all cases during etching processes can be simply handled in this way using table 1. To solve this problem, a method, similar to 'interpolation', is developed. The anisotropic etching rate of silicon obeys the Boltzmann distribution [44]

$$R = R_0 \, \mathrm{e}^{-\Delta E / k_B T}, \tag{5}$$

where R stands for the silicon etching rate, R_0 is a pre-exponential factor, k_B is the Boltzmann constant, T is the temperature and ΔE stands for the effective activation energy. Since the main high index planes have been determined according to table 1, 'interpolation' is only used to handle some other cases for the implementation of silicon anisotropic

etching process simulation. Based on the theory given by equation (5), the interpolation method to calculate the anisotropic etching rates of surface cells can be expressed as

$$R = R_{\text{plane}} \exp(-e_1(n - n_1) - e_2(m - m_1)/k_B T), \qquad (6)$$

where R_{plane} stands the etching rate of a surface cell on a typical plane as given by table 1, n and m are the numbers of second nearest surface and interior neighbors of the target surface cell, n_1 and m_1 are the numbers of second nearest surface and interior neighbors of a surface cell on a typical plane as given by table 1. Whether one plane should be considered as the typical plane corresponding to a target surface cell depends on the numbers of the first nearest surface and interior neighbors of this target cell. For example, if the cell type of a surface cell the cell type is (2s, 1i, 2s, 5i), then the cell locates on the (1 1 0) plane, and its etching rate can be calculated using the method above. However, if the cell type of a surface cell is (2s, 1i, 4s, 3i), the cell locates on the (3 3 1) plane and its etching rate is then calculated also using the method above. If the cell type of a surface cell is (2s, 1i, 4s, 2i), then the cell locates on other planes not listed in table 1. In this model, we will calculate the etching rate of the surface cell in this situation using equation (6). The parameters are as follows: R_{plane} stands for the microscopic etching rate of a surface cell located on the (1 1 0) plane, n, m, n_1 and m_1 are 4, 2, 5 and 2, respectively. Parameters e_1 and e_2 are adopted to describe different effects from the second nearest surface neighbors and the second nearest interior neighbors on the microscopic etching rate (the effective activation energy) of a surface cell. This also means that the contributions from the second nearest surface neighbors and the second nearest interior neighbors to the total bond energy of the target cell are different. The ratio of e_2 and e_1 is

$$H = \frac{e_2(\text{eV})}{e_1(\text{eV})}. \qquad (7)$$

In our approaches, a proper value of H is found to be about 1.18, determined by various comparisons of the experimental and simulation profiles. Theoretically speaking, if the effects from the indirect second nearest neighbors and the direct second nearest neighbors can be independently considered, the accuracy of the model can be improved according to the researches by Gosalvez *et al* [19, 31]. However, this will lead to complex fitting procedures, so this method is not selected in our present approaches.

Although this 'interpolation' method seems to be a very arbitrary choice, it works well in our simulations. One possible reason is that some typical planes occurring during the etching processes have been accurately determined, so the inaccuracy caused by the 'interpolation' for some other crystal planes is not so significant. Another possible reason is that the parameters for the 'interpolation' have been adjusted according to the agreement level of various simulation results and the corresponding experimental results, so the inaccuracy of the 'interpolation' has been efficiently reduced.

Based on the available macroscopic etching rates for different crystal planes in KOH solution, some simulations have been carried out to investigate the effectiveness of our approaches. The simulations are implemented with different orientation silicon wafers which are individually etched in KOH solution; thus the macroscopic etching rates for these wafers can be determined directly [49]. Figure 6 shows the macroscopic etching rates from simulations for some typical crystal planes in 30 wt%, 40 wt% and 50 wt% KOH solution, and the corresponding available experimental results have been compared with the simulation results [43, 45]. The dash lines indicate the etching rates from our simulations and the solid lines indicate the etching rates from available experiments. The parameters are divided into two groups and respectively listed in figures 6(*a*) and (*b*), in case the figures are over-crowded. Since the microscopic etching rates of surface cells on (1 0 0), (1 1 0) and (1 1 1) planes are calculated almost directly from the macroscopic etching rates of the corresponding crystal planes, the simulation results should always be the same as those from the corresponding experimental results, if the error accumulation during the simulations can be neglected. Figure 6 shows that the etching rates from simulations for (1 0 0), (1 1 0) and (1 1 1) planes are almost the same as those from experiments. This indicates that the time compensation method presented by Zhu and Liu [12] is effective to reduce the error accumulation during the anisotropic etching process simulation. For other planes, the simulation results are also in good agreement with the experimental results, and this indicates the effectiveness of our CA model for silicon anisotropic etching process simulations.

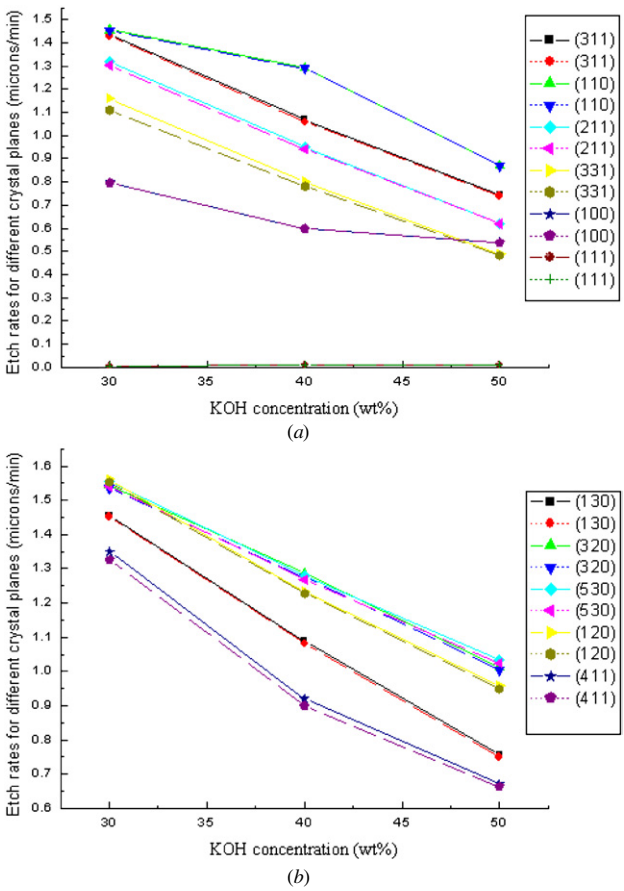

Figure 6. Comparisons of experimental and simulation etching rates for some typical crystal planes in 30 wt%, 40 wt% and 50 wt% KOH solution.

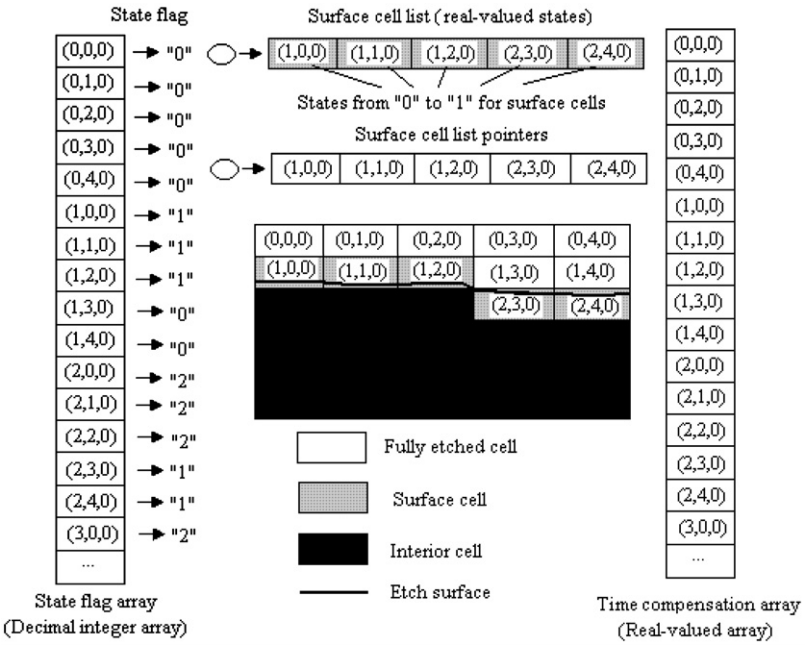

Figure 7. Schematic diagram of the data structure and memory usage of the 3D dynamic CA model.

Generally speaking, there is always a trade-off between the simulation speed and accuracy in the CA modeling method, so it is important to develop an efficient algorithm for our CA model to speed up the simulation while keeping the simulation accuracy. In the next part, an efficient dynamic algorithm will be presented for this requirement.

3. The dynamic CA algorithm

Dynamic algorithms have been reported for several years and have been successfully used in some simulation areas such as lithography, deposition and etching simulations [46–48]. The ideas to incorporate dynamic algorithms into the silicon anisotropic etching simulation have been introduced for several years [8]. Recently, a dynamical continuous CA model has been successfully developed for silicon anisotropic etching simulations by Zhu and Liu [12]. By using a dynamic algorithm, only the boundary cells are processed, so that the simulation speed is significantly improved. In this paper, we present a dynamic algorithm matched with our continuous CA model to reduce memory usage and to speed up the simulation of silicon anisotropic etching processes.

In the continuous CA model, surface cells can have continuous state variables, ranging from '0' (fully etched) to '1' (unetched) [12]. An interior cell that has at least one fully etched first nearest neighbor becomes a boundary cell. In order to capture the 3D etching profiles with less memory usage, state flag array (decimal integer flag F), but not state array (real-valued array), is adopted to indicate the relations between cells and the etching surface.

- $F = 0$ indicates that the cell is fully etched.
- $F = 1$ indicates that the cell is a surface cell, namely at least one of the first nearest neighbors is fully etched.
- $F = 2$ indicates that the cell is an interior cell, namely none of the first nearest neighbors is fully etched.

A 3D state flag array, a surface cell list storing the real-valued states of the surface cells, and a corresponding linked list of surface cell pointers (integer pointers) are used for the implementation of the dynamic algorithm based on our 3D continuous CA model, as shown in figure 7. At the beginning of the simulation, the silicon wafer is divided into 3D silicon crystal structure, and all cells are in state flag '2' (unetched) in the corresponding 3D state flag array. Initial conditions are imposed by changing the state flag of some cells, on the etching window, from '2' to '1'. The surface cell list will be constructed by these cells which are allocated with the real-valued state '1', and the corresponding pointers to these surface cells will also be constructed; thus the anisotropic etching process can start along the etching surface cells. During the course of etching simulation, some surface cells will gradually become fully etched and those fully etched cells will be excluded from the surface cell list, and their corresponding state flag, in the 3D state flag array, will change from '1' to '0'. And also, since the time compensation method [12] is adopted to increase the simulation accuracy, the corresponding respective time compensation values for those fully etched surface cells during the current etching step will be calculated for the etching simulation of their neighbor cells in the next time step. At the same time, some interior cells will become surface cells according to the CA rules and these new surface cells will be inserted into the surface cell list and the corresponding pointers to these new surface cells will also be created. The corresponding state flag for these new surface cells, in the 3D state flag array, will change from '2' to '1'.

During the etching simulation, the states of the surface cells are determined by the etching calculation according to their respective etching rates from our method introduced in part 2. Which cell will be inserted into the surface cell list or be excluded from the surface cell list can be implemented

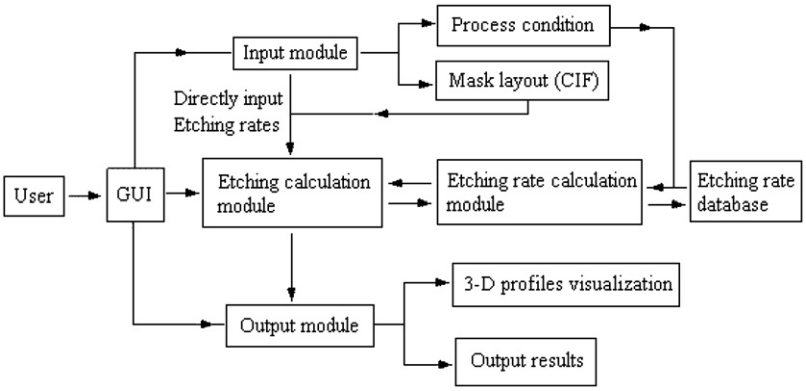

Figure 8. System structure diagram of SEAES.

using the state flag array and the state calculation in the surface cell list, so that only the state flag array, but not the state array, is used in the 3D continuous CA model implemented with the dynamic algorithm (named 3D dynamic CA model) to reduce the memory usage. Generally speaking, the memory elements used to store the etching profiles for the static CA model are more than five times of those for dynamic CA models. In this approach, the memory element usage for the dynamic CA model is further reduced. For the simulation domain of a $100 \times 100 \times 100$ cell array, the storage of 3D etching profiles (3D solid structures) is further reduced from about 8 Mb (cell state in double float data) or 4 Mb (cell state in float data) to 2 Mb (cell state flag in int or short int data) in our CA model, as shown in figure 7.

For the simulation domain of a $200 \times 200 \times 60$ cell array, the total memory usage to implement the anisotropic etching process simulation is about 15.2 Mb for our 3D dynamical CA model. And the typical CPU time for 800 simulation steps for such simulation domain is usually less than 1.1 min on a Pentium IV machine. Note that, compared with the above memory usage, if only the etching surface profiles, but not the 3D solid structures, are expected to be stored, the required memory elements will be significantly reduced as reported in ACES [12]. Since we want to carry out some mechanical analysis of the simulation profiles using finite element analysis tools or CA methods in the future, the 3D solid structures of simulation are expected to be stored.

4. SEAES system

Based on the 3D dynamic CA model, combining the 3D continuous CA model with the dynamic algorithm, a new PC-based 3D anisotropic etching simulator named SEAES has been developed to predict the etching profiles. Besides (1 0 0), (1 1 0), (1 1 1), high index planes such as (2 1 1), (3 1 1), (3 3 1) and (4 1 1) are successfully incorporated into the anisotropic etching simulation system.

The structure of the simulation system is given in figure 8. The input and output modules are connected to the graphical user interface (GUI). The input module is used to input process conditions, mask layout, and sometimes the macroscopic etching rates for different crystal planes if a user chooses the 'direct input' method for etching rate specification; thus the user can input the favorite macroscopic etching rates for different crystal planes and they are advised to consult our macroscopic etching rate database before doing that. The output module describes the etching profiles and visualizes the etching results. The etching rate database, which are being improved, is used to provide the etching rates for different crystal planes according to the inputted process conditions if the user chooses 'indirect input' method for etching rate specification. Since the etching calculation module is based on CA, complex anisotropic etching process simulations using different mask patterns can be easily implemented by SEAES.

Although the 3D dynamic CA model is not very convenient since it requires nine inputted parameters (etching rates for nine typical silicon crystal planes), it can satisfy the requirements of many engineering practice cases. A novel model with both some reasonable physical and chemical points [50], based on some recent work [19], are scheduled to be incorporated into the simulator with less parameters needed to be inputted. This is also believed to be useful to make the simulator suitable for various users with different backgrounds.

5. Simulations and discussions

SEAES has been adopted to carry out a series of silicon anisotropic etching simulations to investigate the effectiveness of the 3D dynamic CA model. The mask shapes for simulations are input into SEAES in CIF format. In this section, we present a series of simulation results on a silicon (1 0 0) wafer using KOH solution, and the simulation results will be compared with the corresponding experimental results.

At first, a mask with three rectangular etching openings with different orientation misalignments to the ⟨1 1 0⟩ direction, as shown in figure 9(*a*), is adopted. Note that, the mask type is dark, and in SEAES, dark mask means that the figures you draw will be exposed to etching solutions during the anisotropic etching processes. The temperature of KOH solution is 70 °C and the concentration of KOH solution is 40 wt%. Figure 9(*b*) is the simulation result corresponding to the etching time of 50 min, and the simulation results is in

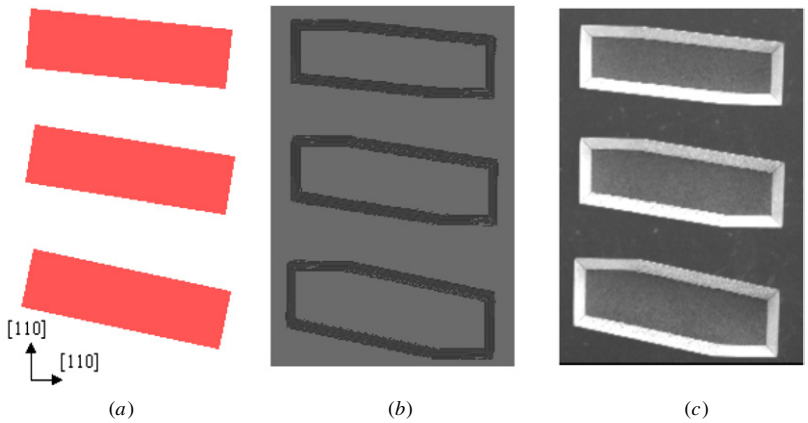

Figure 9. Comparisons of simulation and experimental results using a mask with three rectangular etching openings with different orientation misalignments to the ⟨1 1 0⟩ direction: (*a*) mask shape, (*b*) simulation results for 50 min etching and (*c*) experimental results corresponding to (*b*).

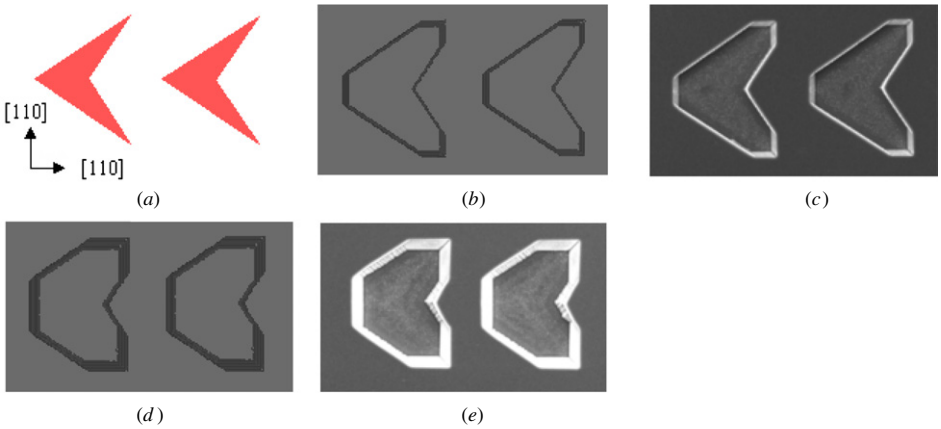

Figure 10. Comparisons of simulation and experimental results using a special mask shape on a (1 0 0)-oriented wafer: (*a*) mask shape, (*b*) simulation results for 30 min etching, (*c*) experimental results corresponding to (*b*), (*d*) simulation results for 50 min etching and (*e*) experimental results corresponding to (*d*).

good agreement with the corresponding experimental result, as shown in figure 9(*c*). With the etching continues, the slow-etching {1 1 1} plane becomes revealed and will dominate the etching process for the mask shape in figure 9(*a*). The etching process for non-convex corners will be dominated by crystal planes with low etching rates such as {1 1 1} planes, while for the etching process of convex corners will be dominated by crystal planes with high etching rates, such as {4 1 1} and {2 1 1} planes [51]. This will be further validated by the following simulations and experiments.

Mask shapes as shown in figure 10(*a*) are then adopted, and the mask type is also dark. The temperature of KOH solution is 70 °C and the concentration of KOH solution is 40 wt%. Figures 10(*b*) and (*d*) are the simulation results corresponding to the etching time of 30 min and 50 min, respectively. The simulation results are found to be in good agreement with the corresponding experimental results, as shown in figures 10(*c*) and (*e*), respectively. After that, another specially designed mask shape as shown in figure 11(*a*) is adopted to further investigate the effectiveness of the 3D dynamic CA model. The mask type is also dark and the etching conditions keep unchanged as above. The simulation results are also in good agreement with the corresponding experimental results, as shown in figures 11(*b*) and (*c*).

The convex corner etching with or without compensation structures is very useful to evaluate the efficiency of an anisotropic etching simulation model for various high index planes that appear during the etching process. The anisotropic etching process of convex corner in 30 wt% KOH solution with a compensation structure [52] is successfully simulated by the simulator. Figures 12(*a*)–(*d*) are the simulation profiles corresponding to the etching time of 120, 230, 345 and 420 min, respectively. The simulation results show an agreement with the available experimental results [52]. As shown in figure 12, the high index planes occurring during the etching process are successfully predicted by the simulations.

Though the resolution of the physical mask is limited, a spoke pattern [53] is widely used to obtain the etching rate as a function of orientation. For the spoke mask shape as given by figure 13(*a*), the corresponding simulation result of the anisotropic etching process in 40 wt% KOH solution is shown in figure 13(*b*). It matches well with the corresponding experimental results, as shown in figure 13(*d*). Comparing

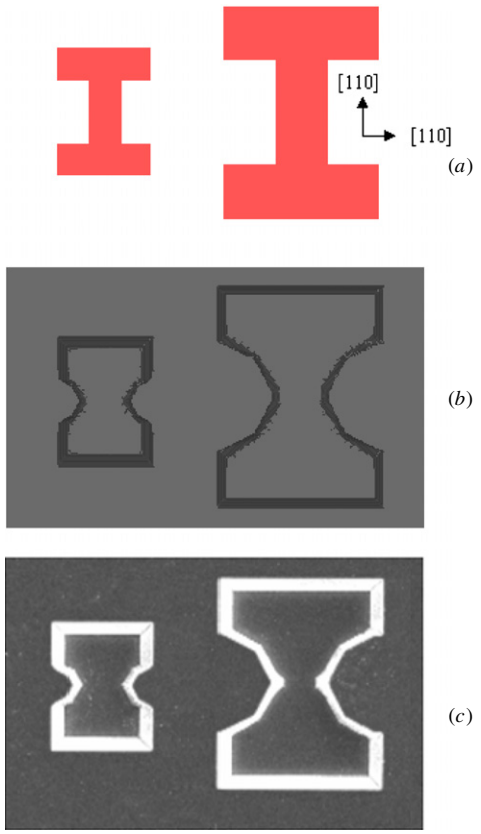

Figure 11. Comparisons of simulation and experimental results for silicon anisotropic etching in KOH solution: (*a*) mask shape, (*b*) simulation results for 50 min etching, (*c*) experimental results corresponding to (*b*).

the simulation result by using Beta2 of ACES [12, 54] with the same etching rate data for (1 0 0), (1 1 0), (1 1 1) and (3 1 1) planes (The etching rates for (1 0 0), (1 1 0), (1 1 1) and (3 1 1) planes are 0.599 μm min^{-1}, 1.294 μm min^{-1}, 0.009 μm min^{-1} and 1.067 μm min^{-1}, respectively [43].), as shown in figure 13(*c*), the result from SEAES is more approximated to the experimental result, for more crystal planes have been accurately incorporated. Thus the 3D dynamic CA model becomes more effective to simulate the silicon anisotropic etching processes. Note that there is still some difference between the experimental and simulation results, because some high index planes have not yet been accurately incorporated into the 3D continuous CA model. In this simulation, the simulation domain is a 600 $\times$ 600 $\times$ 10 cell array, and the typical CPU time is about 1.5 min on a Pentium IV machine.

Finally, the mask shape with two rectangular etching windows is adopted and the edges of the etching windows are aligned to the $\langle 1\,0\,0 \rangle$ direction. The concentration of KOH solution is changed to 30 wt% and the temperature is changed to 80 °C. After the etching begins, the {1 1 1} planes occur in the corners of the etching windows and dominate the etching process, as shown in figure 14(*a*). Because the two etching windows are close to each other, the respective 3D etching profiles corresponding to the two etching windows become merged with the increasing etching time, as shown in figure 14(*c*). The simulation results are in good agreement

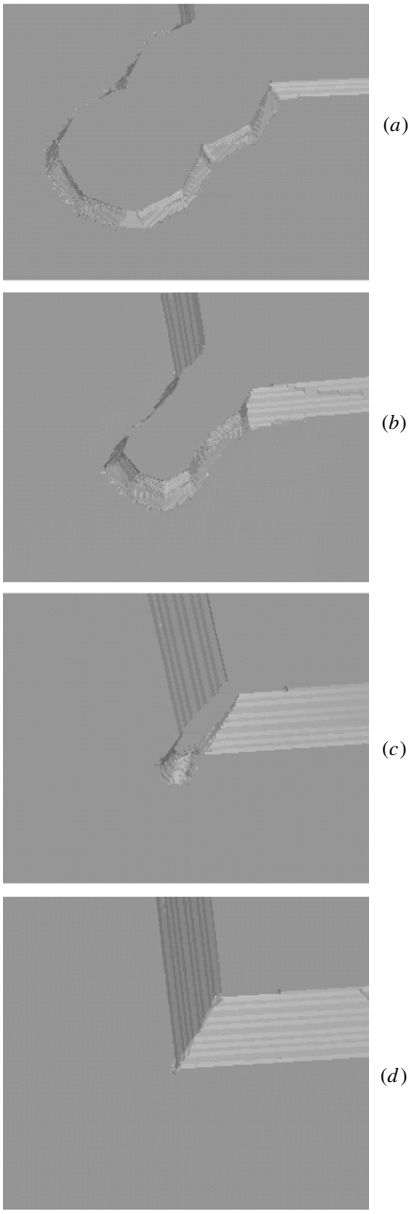

Figure 12. Simulation results for convex corner etching in KOH solution with compensation structures: (*a*), (*b*), (*c*) and (*d*) are the etching results corresponding to the etching time of 120 min, 230 min, 345 min and 420 min, respectively.

with the corresponding experimental results, as shown in figures 14(*b*) and (*d*).

From the simulation results, we can see that the dynamic CA model is not only accurate to predict the etching profiles with non-convex corner etching processes, but also suitable to predict the etching profiles with convex corner etching processes, and the arbitrarily complex mask shapes and the merging of 3D etching profiles can be both efficiently and accurately handled. The above simulation results also show that the simulation results by SEAES are in good quantitative agreement with the experimental results. This indicates the effectiveness of the 3D continuous CA model and the dynamic algorithm for silicon anisotropic etching simulations.

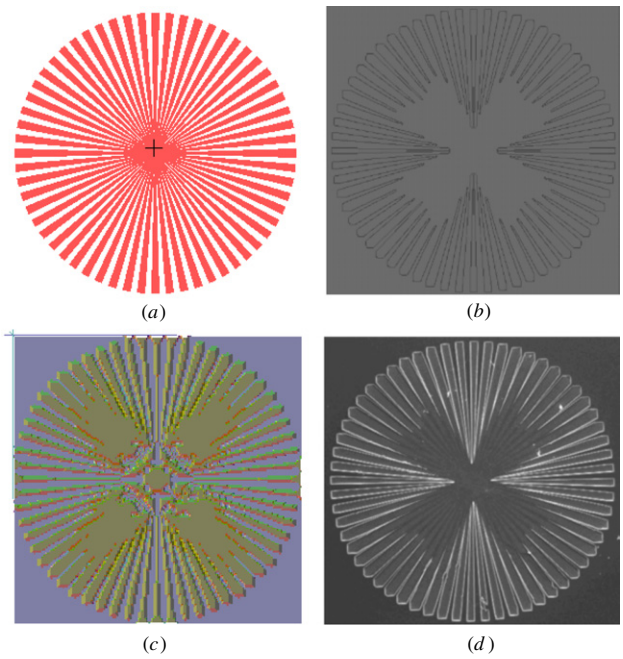

Figure 13. Comparison of simulation and experimental results using a spoke mask in KOH solution: (*a*) mask shape, (*b*) simulation result by SEAES, (*c*) simulation result by ACES, and (*d*) experimental result.

6. Conclusions

A novel 3D continuous CA model has been presented with high index planes such as (2 1 1), (3 1 1), (3 3 1) and (4 1 1) are efficiently incorporated. A dynamic algorithm has also been developed to speed up the simulation process and reduce the memory usage. A 3D silicon anisotropic etching simulator has been implemented based on the 3D continuous CA model and the dynamic algorithm. A series of simulations have been implemented to investigate the effectiveness of our CA model and the dynamic algorithm. The simulation results by SEAES have been found to be in good agreement with the experimental results. A novel model with both some reasonable physical and chemical points, based on some recent work, are scheduled to be incorporated into the simulator. This is identified to be useful for the research of anisotropic etching technologies and the development of MEMS design.

Acknowledgments

The authors gratefully acknowledge Dr M A Gosalvez from the Department of Micro-Nanosystem Engineering of Nagoya University of Japan for some helpful discussions and suggestions. They also extend their sincere appreciation to Professor Fei-Peng Da and Hai-Ping Shen from the Southeast University of China for their help during the simulation

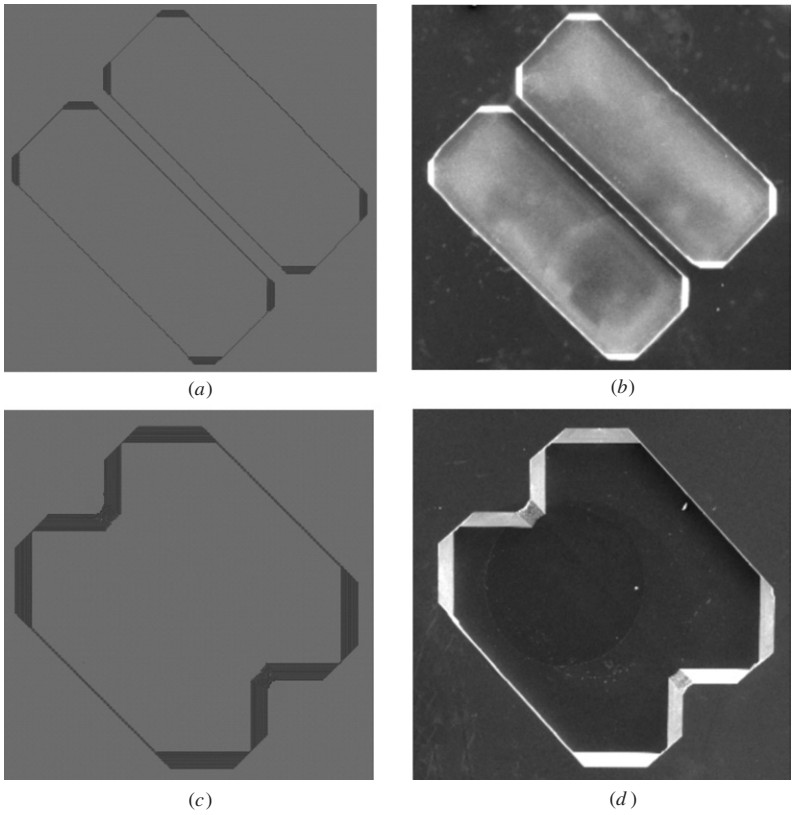

Figure 14. Simulation and experimental results using two rectangular etching openings with the edges aligned to the ⟨1 0 0⟩ direction: (*a*) and (*c*) are the simulation results corresponding to the etching time of 42 min and 100 min, respectively, (*b*) and (*d*) are the experimental results corresponding to (*a*) and (*c*), respectively.

result visualization. The project is supported by the National Nature Science Foundation of China under Contract NSFC-50325519.

References

[1] Bean K E 1978 *IEEE Trans. Electron Devices* **ED-25** 1178–85
[2] Petersen K E 1982 *Proc. IEEE* **70** 420–57
[3] Buser R A and Rooij N F 1991 *Sensors Actuators* **28** 71–8
[4] Danel J S and Delapierre G 1992 *Sensors Actuators* **31** 267–74
[5] Fruehauf J *et al* 1993 *J. Micromech. Microeng.* **3** 113–5
[6] Asaumi K, Iriye K and Sato K 1997 *Proc. IEEE MEMS'97 (Nagoya, Japan)*
[7] Li G, Hubbard T and Antonsson E K 1998 *IEEE MSM'98 (Santa Clara, USA)*
[8] Than O and Buttgenbach S 1994 *Sensors Actuators* A **45** 85–8
[9] Hubbard T and Antonsson E K 1997 *Sensors Mater.* **19** 437–48
[10] Marchetti J *et al* 1998 *SPIE Symp. on Micromaching and Microfabrication, Micromachinged Devices and Components (Santa Clara, USA)*
[11] Nishidate K, Baba M and Gayload R 1998 *Comput. Phys.* **12** 88–93
[12] Zhu Z and Liu C 2000 *J. Microelectromech. Syst.* **9** 252–61
[13] Camon H and Moktadir Z 1996 *Microeletron. J.* **28** 509–17
[14] Kakinaga K *et al* 2004 *IEEJ Trans. SM* **124** 7–13
[15] Gosalvez M A *et al* 2001 *Appl. Surf. Sci.* **178** 7–26
[16] Camon H and Moktadir Z 1995 *Sensors Actuators* A **46–47** 27–9
[17] Hajela P and Kim B 2001 *Struct. Multidiscip. Optim.* **23** 24–33
[18] Kita E and Toyoda T 2000 *Struct. Multidiscip. Optim.* **19** 64–73
[19] Gosalvez M A, Foster A S and Nieminen R M 2002 *Appl. Surf. Sci.* **202** 160–82
[20] Allongue P, Costa-Kieling V and Gerischer H 1993 *J. Electrochem. Soc.* **140** 1009–18
[21] Allongue P, Costa-Kieling V and Gerischer H 1993 *J. Electrochem. Soc.* **140** 1018–26
[22] Kasparian J, Elwenspoek M and Allongue P 1997 *Surf. Sci.* **388** 50–62
[23] Van Veenendaal E *et al* 2001 *Sensors Actuators* A **93** 219–31
[24] Flidr J *et al* 1998 *J. Chem. Phys.* **108** 5542–53
[25] Hines M A 2001 *Sensors Mater.* **13** 247–59
[26] Wind R A and Hines M A 2000 *Surf. Sci.* **460** 21–38
[27] Allongue P 1996 *Phys. Rev. Lett.* **77** 1986–9
[28] Seidel H 1990 *IEEE Transducers '90 (New York, USA)*
[29] Seidel H *et al* 1990 *J. Electrochem. Soc.* **137** 3626–32
[30] Gosalvez M A 2006 private communication
[31] Gosalvez M A, Foster A S and Nieminen R M 2002 *Europhys. Lett.* **60** 467–73
[32] Zubel I 2001 *Sensors Actuators* A **94** 76–86
[33] Seidel H, Heuberger C A and Baumgarel H 1990 *J. Electrochem. Soc.* **137** 3612–26
[34] Shikida M *et al Proc. IEEE MEMS '99 (Orlando, USA)*
[35] Tokoro K *et al* 1998 *Proc. IEEE MHS '98 (Nagoya, Japan)*
[36] Yang C R *et al* 2005 *Sensors Actuators* A **199** 271–81
[37] Merlos A *et al* 1993 *Sensors Actuators* A **37–38** 737–43
[38] Sonphao W and Chaisirikul S 2001 *Proc. ISIE1'2001 (Ladkrabang, Thailand)*
[39] Sato K *et al* 1998 *Proc. IEEE MEMS '98 (Heidelberg, Germany)*
[40] Steinland E *et al* 1996 *Sensors Actuators* A **54** 728–32
[41] Tabada O *et al* 1992 *Sensors Actuators* **34** 51–7
[42] http://www.virginiasemi.com/pdf/siliconetchingandcleaning.pdf
[43] Yamamoto M *et al* 1998 *Sensors Actuators* A **64** 87–93
[44] Jiang Y F and Huang Q A 2005 *Semicond. Sci. Technol.* **20** 524–31
[45] Enokssony P 1997 *J. Micromech. Microeng.* **7** 141–4
[46] Scheckler E W *et al* 1993 *IEEE Trans. Comput.-Aided Des. Integr. Circuit Syst.* **12** 1345–56
[47] Huang Q A *et al* 2006 *J. Micromech. Microeng.* **16** 1–8
[48] Zhou Z F *et al* 2005 *J. Micromech. Microeng.* **15** 652–62
[49] Gosalvez M A 2006 private discussions
[50] Zhou Z F *et al* 2006 in preparation
[51] Liu C 2006 *Foundations of MEMS* (Englewood Cliffs, NJ: Prentice-Hall)
[52] Fan W and Zhang D C 2006 *J. Micromech. Microeng.* **16** 1951–7
[53] Hubbard T and Antonsson E K 1994 *J. Microelectromech. Syst.* **3** 19–28
[54] http://mass.micro.uiuc.edu/research/completed/aces/pages/home.html